JOURNAL OF AIRCRAFT
Vol. 47, No. 2, March–April 2010

Aerodynamic–Structural Design Studies of Low-Sweep Transonic Wings

Antony Jameson*
Stanford University, Stanford, California 94305-3030
John C. Vassberg†
Hydro-Aero Consulting Group, Long Beach, California 90803
and
Sriram Shankaran‡
Intelligent Aerodynamics, Menlo Park, California 94325

DOI: 10.2514/1.42775

The current generation of wing designs for civilian air transport typically have a swept wing. However, these wings were designed without the aid of modern high-fidelity simulation and multidisciplinary optimization tools. With rapid advances in numerical simulation of high-Reynolds-number flows and efficient shape-optimization techniques, it is now possible to revisit the designs of modern commercial wide-body aircraft to quantitatively and qualitatively determine the sweep of transonic wings. Results from the aerodynamic shape optimization of a low-sweep wing of a modern transonic civil transport aircraft shows that it is possible to delay the drag rise of this wing to beyond Mach Number of 0.8 if the sections are redesigned. It is conceivable that future aircraft designs will be governed by the need to deliver improved performance with reduced fuel consumption. In this study, we systematically study the feasibility of designing wings with low sweep without aerodynamic or structural performance penalties. The study presented here explores the possibility of extending some commonly accepted limits related to the general layout of an efficient transonic wing. Specifically, the Mach–sweep–thickness relationships are revisited at a cursory level. Pure aerodynamic optimization of wings with varying sweeps (5 to 35 degrees) shows that the design space is relatively flat. These optimized configurations are then studied using an aerostructural optimization package along with planform variations. The aerostructural optimization reveals that the design space is again relatively flat, confirming the assumption that wings with low sweep can be effectively used as an alternative to current sweptback configurations. The results obtained from the optimization studies show that it may be possible to significantly reduce wing sweep without incurring either aerodynamic or structural penalties, especially for $M \leq 0.8$ aircraft designs.

Nomenclature

Ar	=	wing aspect ratio
b	=	wing span
C	=	wing chord
C_D	=	drag coefficient
C_W	=	wing weight coefficient
$E(\rho)$	=	Young's modulus
L/D	=	lift-to-drag ratio
M	=	Mach number
p_d	=	target/design pressure
R	=	range
S_{ref}	=	reference area
T	=	wing thickness
u, f_j	=	displacement, force field
W_1	=	takeoff weight
W_2	=	landing weight
α	=	penalty for constraint violation
α_i	=	relative Pareto weights
Λ	=	wing sweep
λ	=	wing taper
ρ	=	density of the material
σ	=	stress on the material

Presented as Paper 0145 at the 46th Aerospace Sciences Meeting and Exhibit, Reno, NV, 7–10 January 2008; received 16 December 2008; accepted for publication 16 January 2010.

*Thomas V. Jones Professor of Engineering, Department of Aeronautics and Astronautics. Fellow AIAA.
†Boeing Technical Fellow. Fellow AIAA.
‡Technology Philanthropist.

I. Introduction

THE current generation of civilian transport aircraft are typically designed with a moderately-high-swept wing. However, the planform layouts of these wings were substantially influenced by historical design charts developed decades ago. These design charts were derived and updated from wind-tunnel and flight data collected over the years; they include shifts due to technology levels, such as that introduced by supercritical airfoil sections. Most of the wing geometries that form the basis of these data were designed using cut-and-try methods and augmented with parametric variations of sweep, thickness, lifting condition, and freestream Mach number. More important, this knowledge base was predominantly developed before the advent of modern high-fidelity simulation capabilities and multidisciplinary optimization tools. With rapid advances in the numerical simulation of high-Reynolds-number flows and efficient shape-optimization techniques, it is now feasible to revisit the general layout drivers of transonic-wing planforms for the benefit of future commercial transport aircraft. Specifically, it may be currently possible to extend the accepted bounding limit of the Mach–sweep–thickness ($M\Lambda T$) relationships. Recent results from an aerodynamic shape optimization of a low-sweep wing of a modern transonic transport have shown that it is possible to delay the drag rise of this wing to beyond a Mach number of 0.8.

Driven by escalating fuel costs as well as by environmental concerns, it is highly likely that future aircraft designs will be directed to deliver improved performance with significantly reduced fuel burn per passenger mile, even if it incurs a modest increase in mission block time. For example, a *sweet spot* in the aircraft design space may exist near $M = 0.8$, where an unducted-fan engine could

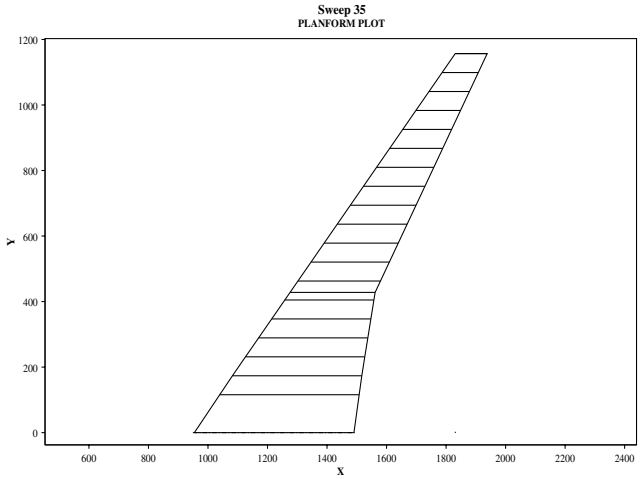

Fig. 1 Planform of baseline $\Lambda = 35°$ wing.

be used, thus yielding large reductions in specific fuel consumption. If it is possible to develop an efficient low-sweep wing capable of $M = 0.8$ cruise, then other synergies such as reductions in manufacturing costs could also be exploited.

In this work, we systematically study the feasibility of designing wings with reduced sweep without incurring aerodynamic or structural performance penalties. Pure aerodynamic optimizations of transonic wings with varying sweeps ($5° \leq \Lambda \leq 35°$) show that the $M\Lambda T$ design space may be relatively flat with respect to ML/D, thus yielding higher range factors at reduced cruise Mach numbers. These aerodynamically optimized configurations were further studied using an aerodynamic–structural optimization package along with planform variations. The aerodynamic–structural optimizations reveal that the $M\Lambda T$ design space remains relatively flat with respect to ML/D and operator empty weight, thus confirming the conclusion that wings with low sweep can be effectively used as an alternative to current higher-sweep configurations.

II. Approach

The approach taken in this study is organized into two phases. In the first phase, pure aerodynamic optimizations were conducted on a parametric variation of wing sweep while holding structural beam properties (lengths and depths) of the exposed wing constant. In the second phase, the aerodynamically optimal wings from the initial phase were reoptimized with a coupled aerodynamic–structural method.

A. Geometry Setup

To establish a consistent set of seed geometries of varying sweep, a baseline wing/body configuration that is typical of current aircraft-design practices was used. This baseline wing/body configuration was developed to cruise efficiently at a Mach number of $M = 0.85$ and a lift coefficient of $C_L = 0.5$; its planform (with defining stations) is depicted in Fig. 1. Figure 2 shows its nondimensional thickness max-T/C (left) and corresponding absolute thickness max-T in inches (right).

Reference quantities are

$$S_{\text{ref}} = 4000 \text{ ft}^2, \qquad b = 192.8 \text{ ft}, \qquad C_{\text{ref}} = 275.8 \text{ in}$$
$$\text{AR} = 9.29, \qquad \lambda = 0.275$$

where S_{ref} is the wing reference area, b is the wing span, C_{ref} is the wing reference chord, $\text{AR} = b^2/S_{\text{ref}}$ is the wing aspect ratio, and λ is the taper ratio of the trap wing. The trap wing of this layout has a quarter-chord sweep of $\Lambda = 35°$. Its side of body is located at 10% semispan, which is at a wing butt-line location of 115.7 in. Its average nondimensional thickness is about 11.5%.

To generate the additional seed wings needed for this investigation, the quarter-chord line of the baseline wing was rotated about its side-of-body location. Each defining airfoil section was simply translated by the movement of its quarter-chord location per the aforementioned rotation. Hence, the absolute dimensions and orientation of each defining airfoil station were not altered relative to the baseline wing. The final modification in establishing the seed wings was to retwist and rerig the wings to provide a similar span-load distribution as that of the baseline wing at a similar fuselage angle of attack. Note that these transformations generate seed wings that retain the structural properties of the baseline wing's beam length and depth. On the other hand, the aerodynamic span, true wing area, and fuel volume all increase accordingly with a reduction in wing sweep. Table 1 gives the variation of wing span as a function of sweep angle. Although the true wing area varies as a result of this transformation, in this study, the wing reference area was held constant and equivalent to that of the baseline wing. Holding wing reference area constant simplifies a drag buildup (described later) that is representative of a complete aircraft.

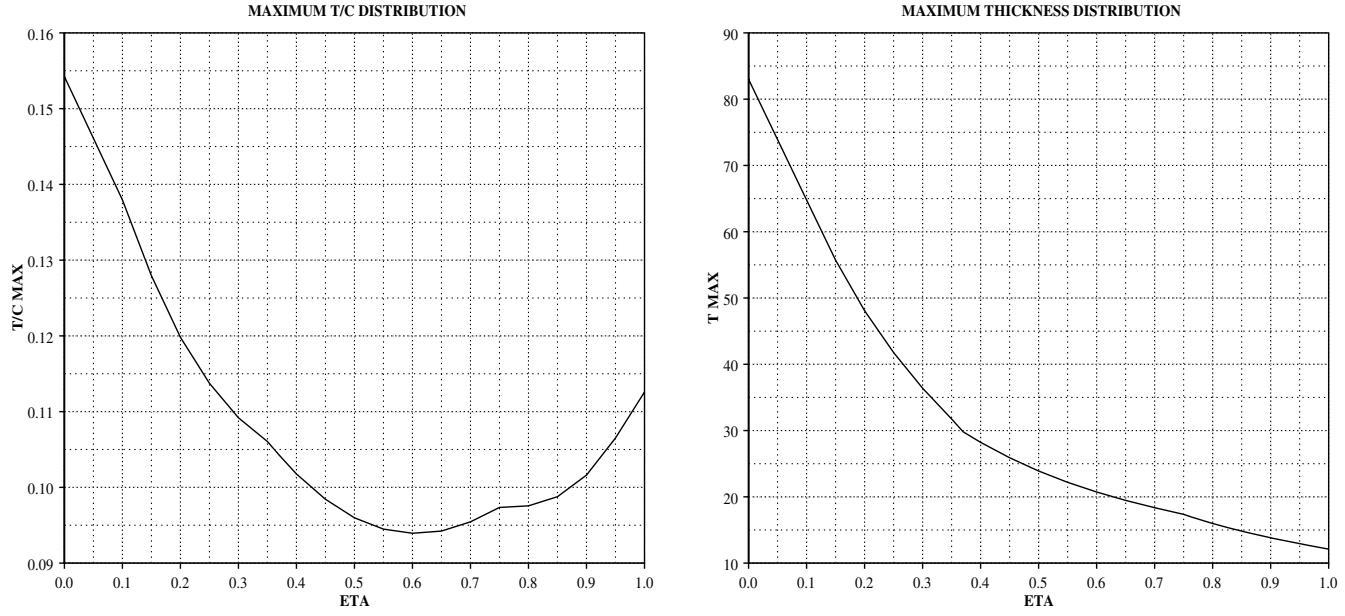

Fig. 2 Nondimensional and absolute (in inches) thickness distributions of baseline $\Lambda = 35°$ wing.

Table 1 Sweep-span relationship of study wings

Sweep	Initial span, ft	A-S[a] span, ft
35°	192.79	193.76
30°	202.72	203.66
25°	211.25	212.30
20°	218.33	218.81
15°	223.88	224.76
10°	227.88	227.76
5°	230.29	229.54

[a]A-S span is the aerodynamic–structural optimized span.

The purpose of setting up the reduced-sweep wings in the above manner was motivated by the desire to have the ability to perform pure aerodynamic optimizations while essentially not impacting wing structural weight. The second phase of our study has verified this underlying assumption.

There are a couple of other items to note. The resulting yehudi regions inboard of the planform break are likely not laid out as they naturally would be in an actual aircraft design. Further, no attempt was made to resize these study wings per real aircraft design considerations. Both of these elements introduce nonoptimal characteristics in the planform layout of the study wings, especially for those with sweep deviating most from that of the baseline. In this respect, the findings herein for the lowest-sweep wings may be overly conservative.

B. Pure Aerodynamic Optimization

The primary goal of the present work was to develop evidence that may challenge the conventional wisdom of what is possible in the $M\Lambda T$ design space for efficient transonic cruise. To accomplish this in a rigorous manner, one would have to comprehensively survey the Mach-C_L space for each of the seven sweep angles under study. This would require on the order of 200 aerodynamic shape optimizations to be performed. Since this level of effort was far beyond the scope of this initial investigation, we instead surveyed the *Mach*-C_L space for the $\Lambda = 10°$ wing to determine reasonable design conditions for this case. We made educated judgements to estimate what flow conditions should be used for the remaining sweep angles. Single-point aerodynamic optimizations were conducted for the remaining sweep angles, starting with each of the seed wings, at their corresponding design conditions. To be consistent with this study, the baseline $\Lambda = 35°$ wing was also reoptimized at its single-point design condition. The shape modifications were constrained to maintain thickness everywhere on the wing, relative to the starting geometries. However, the span-load distribution was allowed to fall out from the optimizations. Note that the aerodynamically optimum span-load for a transonic wing is not necessarily elliptic; e.g., shock and induced drags are traded accordingly. (As it turned out, the span-load distributions of the optimal wings tended to closely match each other without a constraint being applied.)

These aerodynamic optimizations yielded estimates of the minimum drag level possible for each of the wings; simulated as a wing/body configuration. To estimate an absolute drag level for the full configuration aircraft, the wing drag C_D was augmented with an estimate of the drag for the residual aircraft (fuselage, pylons, nacelles, empennage, excrescences, and static trim). This residual drag was taken as $C_{D.\mathrm{res}} = 140$ *counts* relative to the fixed reference area used for all of the study wings; total aircraft drag is then $C_{D.\mathrm{tot}} = C_D + C_{D.\mathrm{res}}$. Based on this rudimentary drag buildup, the quantified metrics of ML/D and $\sqrt{M}L/D$ are representative of the aircraft in flight. Here, ML/D is a measure of aerodynamic performance, and $\sqrt{M}L/D$ is approximately proportional to range factor. According to the Breguet range equation

$$R = \frac{ML}{D}\frac{a}{\mathrm{SFC}}\ell_n\frac{W_1}{W_2}$$

the range efficiency may be estimated by $[(M/\mathrm{SFC})(L/D)]$.

Here, a is the speed of sound, SFC is the specific fuel consumption, and W_1 and W_2 are the takeoff and landing weights, respectively. The SFC of a turbofan engine typically increases with Mach number at a rate that is fairly well approximated by a linear variation with a slope of around 0.5. Accordingly $\sqrt{M}L/D$ may be regarded as a useful indicator of the range factor.

C. Aerodynamic–Structural Optimization

The resulting geometries of the pure aerodynamic optimizations were studied further with a coupled aerodynamic–structural optimization methodology, which explicitly includes the tradeoff between aerodynamic drag and wing structural weight. This explicit tie between aerodynamics and structural weight allowed these optimizations the ability to appropriately vary wing thickness, span, and sweep. However, we note that the finite-element-method-based process used herein is not nearly as rigorous as those employed within a real aircraft-design environment, which include numerous offdesign and flutter conditions scattered throughout the fight envelope, any one of which may size the structure. Specifically, our aerodynamic–structural optimizations were all conducted at single-point cruise conditions and incorporate a surrogate metric of material stress. Here, the allowable material stress distribution is defined by that of the baseline $\Lambda = 35°$ wing. This allowable stress distribution is used during the inner-loop structural optimizations to resize the wing skin thicknesses and therefore provide estimates for the wing structural weights.

To conduct a single-objective aerodynamic–structural optimization, a cost function is developed that blends the coefficient of drag C_D and coefficient of weight C_W together in such a manner as to maximize range while holding Mach number and fuel volume constant.

The following two sections provide an overview of the mathematical developments of both the pure aerodynamic optimization and the aerodynamic–structural optimization methodologies.

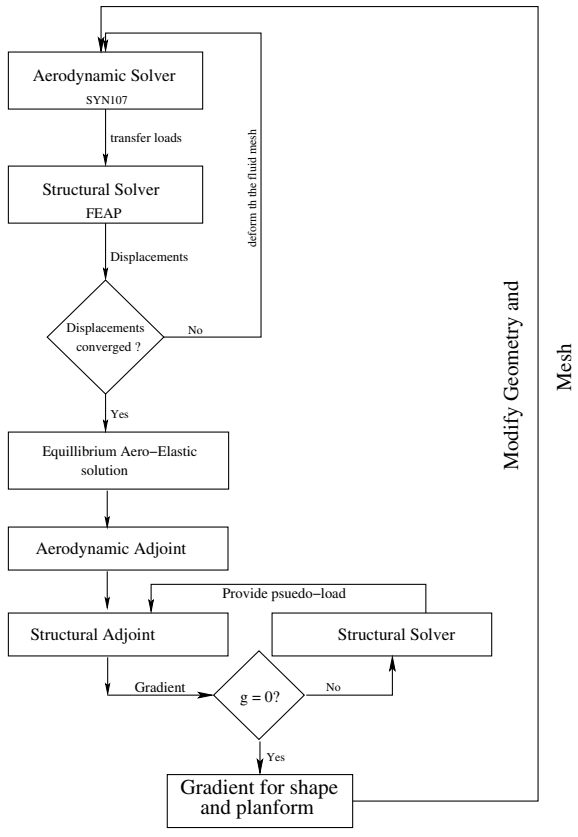

Fig. 3 Overview of aerodynamic–structural design process.

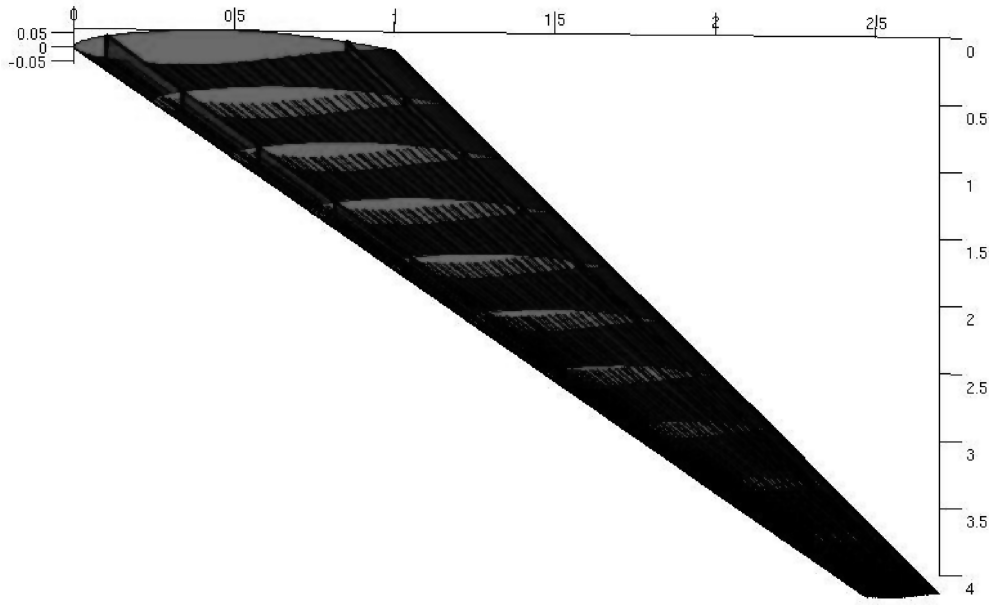

Fig. 4 Cutaway of structural model for wing, showing skin, ribs, spars, and stiffeners.

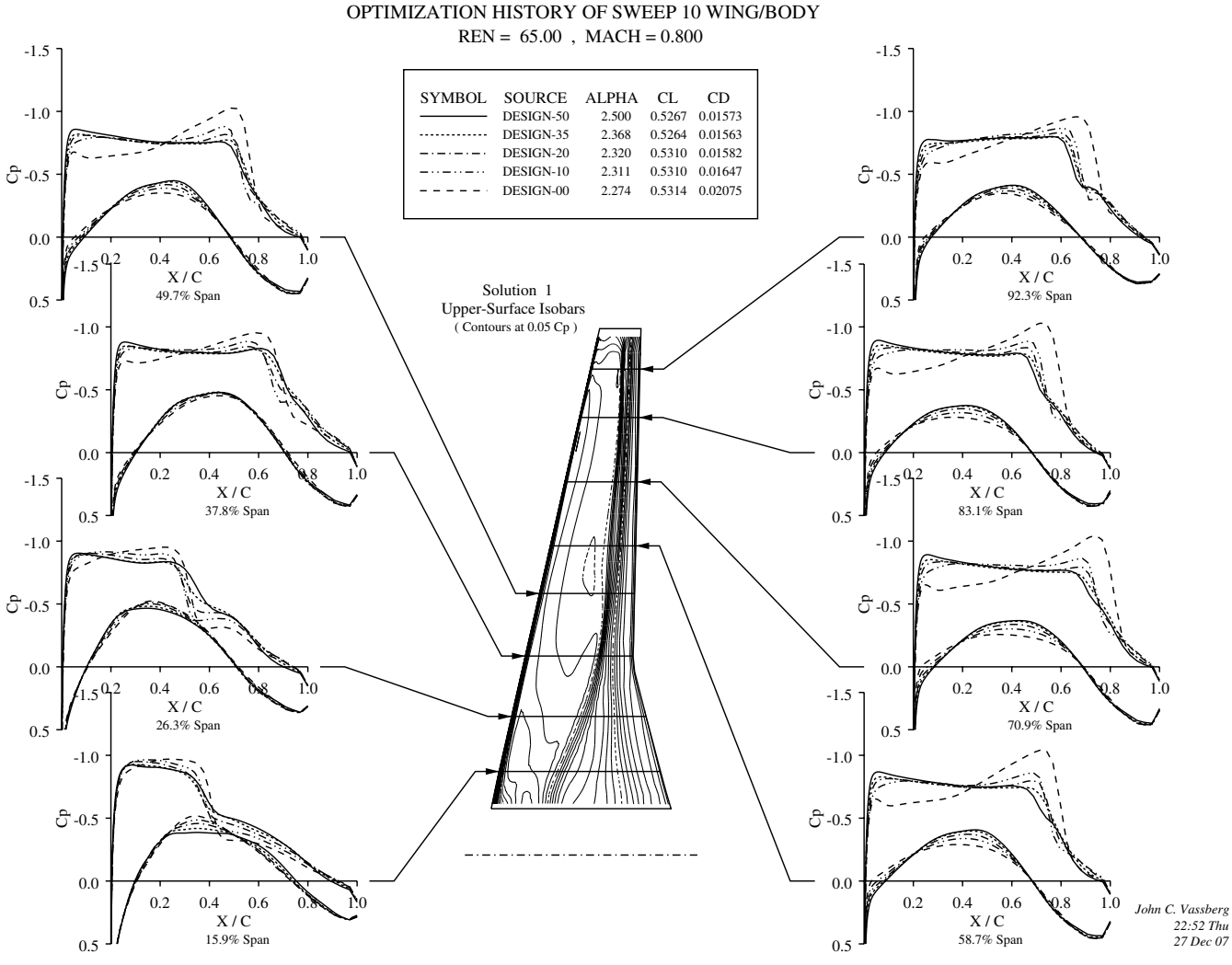

Fig. 5 Evolution of pressures for the $\Lambda = 10°$ wing during optimization.

Table 2 Optimum pure aerodynamic performance[a]

Mach	Sweep	C_L	C_D	$C_{D,\text{tot}}$	ML/D	$\sqrt{M}L/D$
0.85	35°	0.500	153.7	293.7	14.47	15.70
0.84	30°	0.510	151.2	291.2	14.71	16.05
0.83	25°	0.515	151.2	291.2	14.68	16.11
0.82	20°	0.520	151.7	291.7	14.62	16.14
0.81	15°	0.525	152.4	292.4	14.54	16.16
0.80	10°	0.530	152.2	292.2	14.51	16.22
0.79	5°	0.535	152.5	292.5	14.45	16.26

[a]C_D in counts; $C_{D,\text{tot}} = C_D + 140$ counts.

Table 3 Optimum aerodynamic–structural performance[a]

Mach	Sweep	C_L	C_D	C_W	Cost	ML/D	$\sqrt{M}L/D$
0.85	35°	0.500	151.7	0.03562	0.01846	14.57	15.80
0.84	30°	0.510	148.7	0.03531	0.01831	14.84	16.19
0.83	25°	0.515	147.6	0.03537	0.01847	14.86	16.31
0.82	20°	0.520	148.2	0.03500	0.01839	14.80	16.34
0.81	15°	0.525	148.7	0.03465	0.01845	14.73	16.37
0.80	10°	0.530	148.6	0.03464	0.01852	14.69	16.43
0.79	5°	0.535	148.9	0.03455	0.01842	14.63	16.46

[a]C_D in counts, cost $= (\alpha_1 C_D + \alpha_2 C_W)$ maximizes Breguet range, and α_1 is typically set to 1.

III. Aerodynamic Optimization Methodology

The shape-optimization methodology used in this work is based on the theory of optimal control of systems governed by partial differential equations, where the control is by varying the shape of the boundary. We refer the reader to the following references (and references therein) for a detailed review of the method [1–7].

This aerodynamic shape optimization has been applied extensively by the authors over the past 15 years with much success on a wide variety of configurations, including a Reno race plane and a Mars exploration scout [8–11].

IV. Aerodynamic–Structural Optimization Methodology

The importance of interactions between the aerodynamics and the structures is a crucial element in the multidisciplinary design environment that realizes a flight vehicle. Our initial attempts at addressing this issue used the Reynolds-averaged Navier–Stokes equations to model the fluid and a simplified structural model that determined a fully stressed structural layout for the given aerodynamic loads. This approach was further refined to include a detailed finite element model for the wing, consisting of skins, spars, and ribs. Using FEAP, a finite element analysis package developed at the University of California at Berkeley, iterative aeroelastic simulations were performed to realize the static deflected shape.

The optimal structural layout is now determined using the idea of topology optimization [12], which has its basis in optimal control of the equations of static linear elasticity. Typically, an engineer is interested in the design of a structure with minimum weight while satisfying the compliance conditions with respect to the external loads, while also satisfying the constraints on maximum allowable stress. This problem has been widely studied using a discrete adjoint

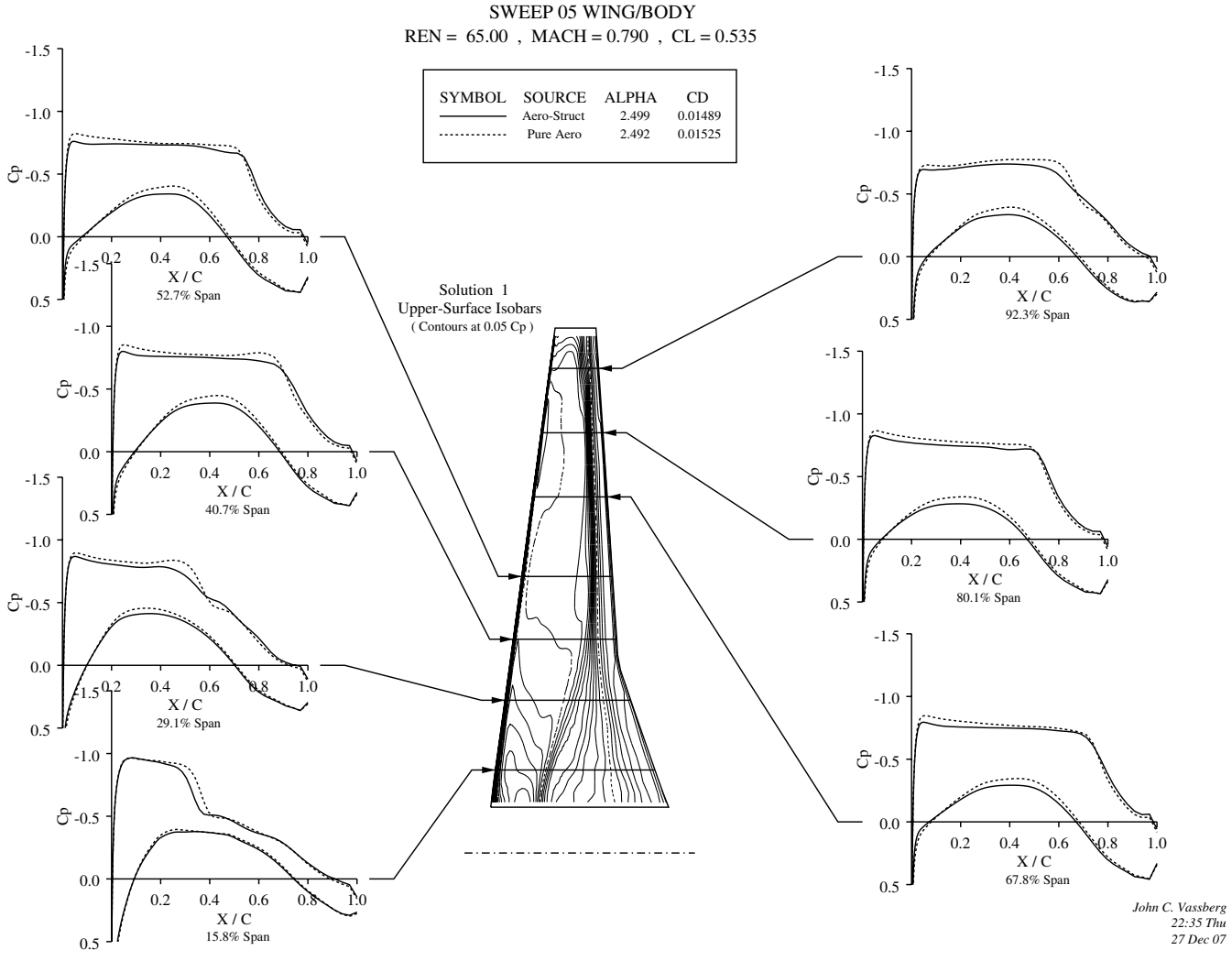

Fig. 6 Optimized design at Mach 0.79 and $\Lambda = 5°$.

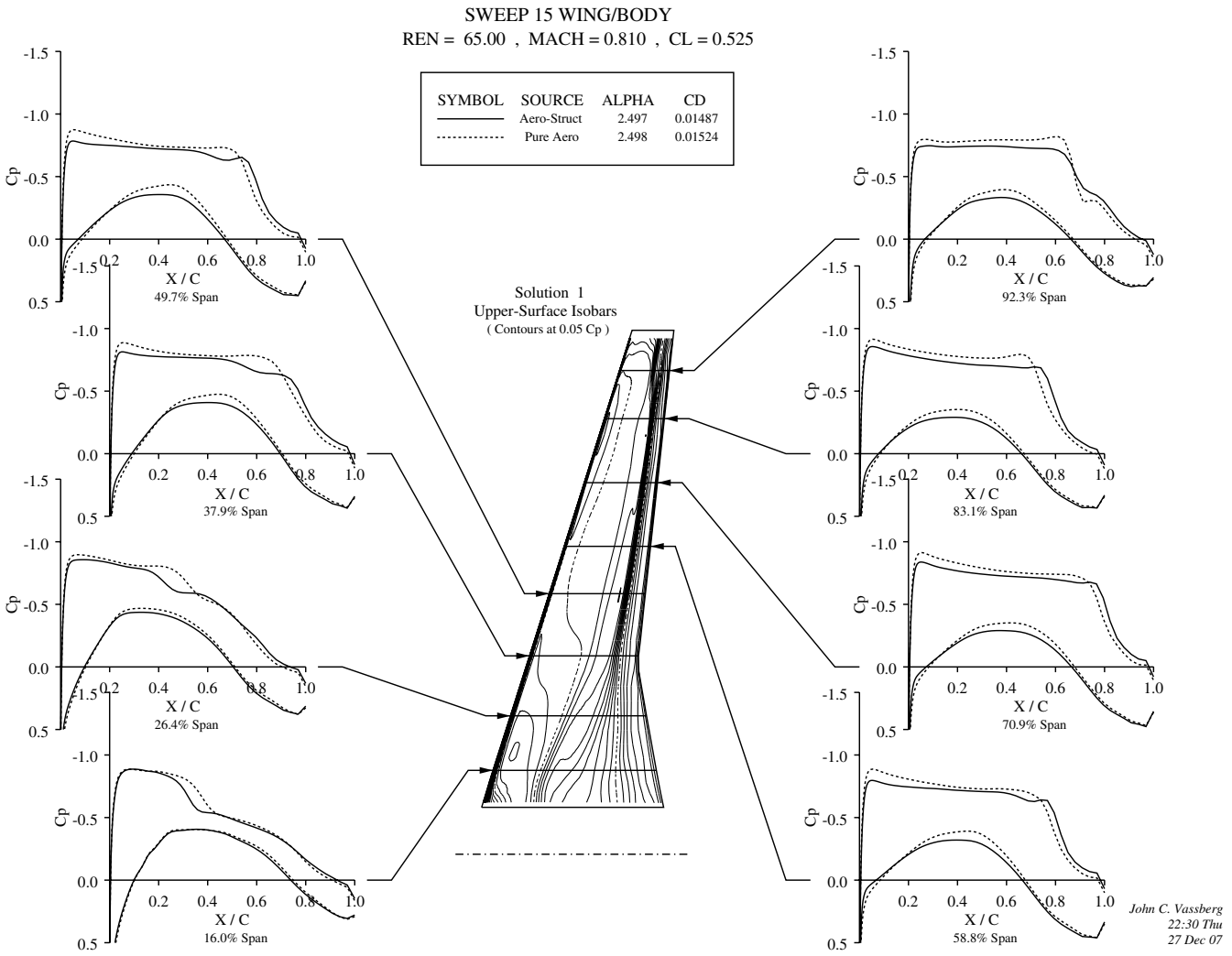

Fig. 7 Optimized design at Mach 0.81 and $\Lambda = 15°$.

formulation in conjunction with the use of a regularizing method that transforms the originally ill-conditioned integer optimization problem to one of continuous optimization. Thus, the optimization problem can be written using a penalty function approach as

$$I(\sigma, \rho) = \int_D \rho \, \mathrm{d}V + \alpha \int_D (\sigma(x^s) - \sigma_{\max})^2 \delta(x^s - x) \, \mathrm{d}V$$

where ρ is the density at each point in the structural domain (D), α is the penalty parameter on the violation of the stress constraints, σ is the stress field in the domain, $\sigma_{\max}$ is the maximum allowable stress, and δ is the Kronecker delta function that enables the inclusion of a domain integral in the objective function for the pointwise stress constraints.

The constraint equations are the governing equations for linear elasticity:

$$\frac{\partial \sigma_{ij}(u)}{\partial x_j} + f_j = 0$$

where f_j are the combined external and internal loads on the structure and u is the displacement field. The optimization problem can now be posed as follows:

$$\min_{\rho} I(\sigma, \rho) \qquad \text{subject to } \sigma_{ij,j} + f_j = 0 \quad \text{and} \quad 0 \le \rho \le 1 \quad (1)$$

Note that the constraint equation is similar in form to the viscous operator for the Navier–Stokes equation. Proceeding in a manner similar to shape optimization for flow problems, we write the variation in the cost function as

$$\delta I = \frac{\partial I}{\partial \sigma} \delta\sigma(u) + \frac{\partial I}{\partial \rho} \delta\rho$$

Table 4 Envelope of optimized drag polars for the 10°-sweep wing at Mach 0.80

C_L	C_D	$C_{D.\text{tot}}$	L/D	C_W	ML/D	$\sqrt{M}L/D$
0.5336	151.5	291.5	18.36	0.03464	14.69	16.42
0.5448	154.0	294.0	18.53	0.03466	14.82	16.57
0.5556	157.5	297.5	18.68	0.03461	14.94	16.71
0.5663	161.1	301.1	18.80	0.03456	15.04	16.82
0.5881	168.6	308.6	19.04	0.03452	15.23	17.03

Table 5 Envelope of optimized drag polars for the baseline 35°-sweep wing at Mach 0.85

C_L	C_D	$C_{D.\text{tot}}$	L/D	C_W	ML/D	$\sqrt{M}L/D$
0.4998	151.4	291.4	17.16	0.03562	14.59	15.82
0.5100	153.3	293.4	17.38	0.03561	14.77	16.02
0.5334	162.2	302.2	17.54	0.03559	14.91	16.17
0.5556	171.9	311.9	17.81	0.03554	15.14	16.42
0.5780	181.2	321.2	17.99	0.03550	15.29	16.59
0.5900	192.9	332.9	17.72	0.03540	15.06	16.34

The variational form of the constraint equations $R(\sigma, \rho) = 0$ for an arbitrary test function ϕ can be written as

$$\int_D \phi \delta R(\sigma, \rho) = 0$$

where

$$\delta R = \frac{\partial R}{\partial \sigma}\delta\sigma + \frac{\partial R}{\partial \rho}\delta\rho$$

Here, the dependence of the constraint equation on the control variable ρ is through the definition of Young's modulus:

$$E(\rho) = \left(\frac{\rho}{\rho_0}\right)^{\beta} E(\rho_0)$$

This regularization enables ρ to vary smoothly between 0 and 1. Integration of the terms in the variational form of the constraint that contain terms corresponding to the variation in the stresses by parts can be written as

$$\int_B \phi \delta\sigma \, \mathrm{d}B - \int_D \frac{\partial \phi}{\partial x_i}\sigma_{ij} \, \mathrm{d}V$$

The first term represents an integral over the boundary of the domain, and the test function on the boundary can be chosen to cancel the term in the variation of the cost function that depends on the variation in the stresses. The second term can be integrated by parts again, after noting that

$$\sigma_{ij} = E(\rho)\frac{\partial u_i}{\partial x_j} \qquad \int_B \frac{\partial \phi}{\partial x} E \delta u_i - \int_D \frac{\partial}{\partial x_i} E \frac{\partial \phi}{\partial x_j}$$

where the first term is identically equal to zero, as the displacements are either prescribed as boundary conditions or as a compliance condition. The second term along with the boundary conditions on the test function along the boundary is the adjoint equation. It has a form similar to the constraint equation (as it is well known that equations of linear elasticity are self-adjoint) and can be solved using the finite element procedure used to obtain the displacement field. Then the cost variation reduces to

$$\int_D \left(1 - \phi^T \frac{\partial}{\partial x_i}\frac{\partial E}{\partial \rho}\frac{\partial u_i}{\partial x_j}\right)\delta\rho \, \mathrm{d}V$$

where the bracketed expression can now be recognized as the gradient. Hence, we can use a similar adjoint approach to determine the sensitivities of a given performance measure with respect to the shape variables and the structural layout to provide a unified approach to concurrently optimize the aerodynamic and structural control variables.

We redesign both wing section and planform to minimize the cost function that is representative of performance metrics in practical design environments. We take convex combinations of the aerodynamic (drag) and structural performance (weight) measures to form a combined metric that can be written as

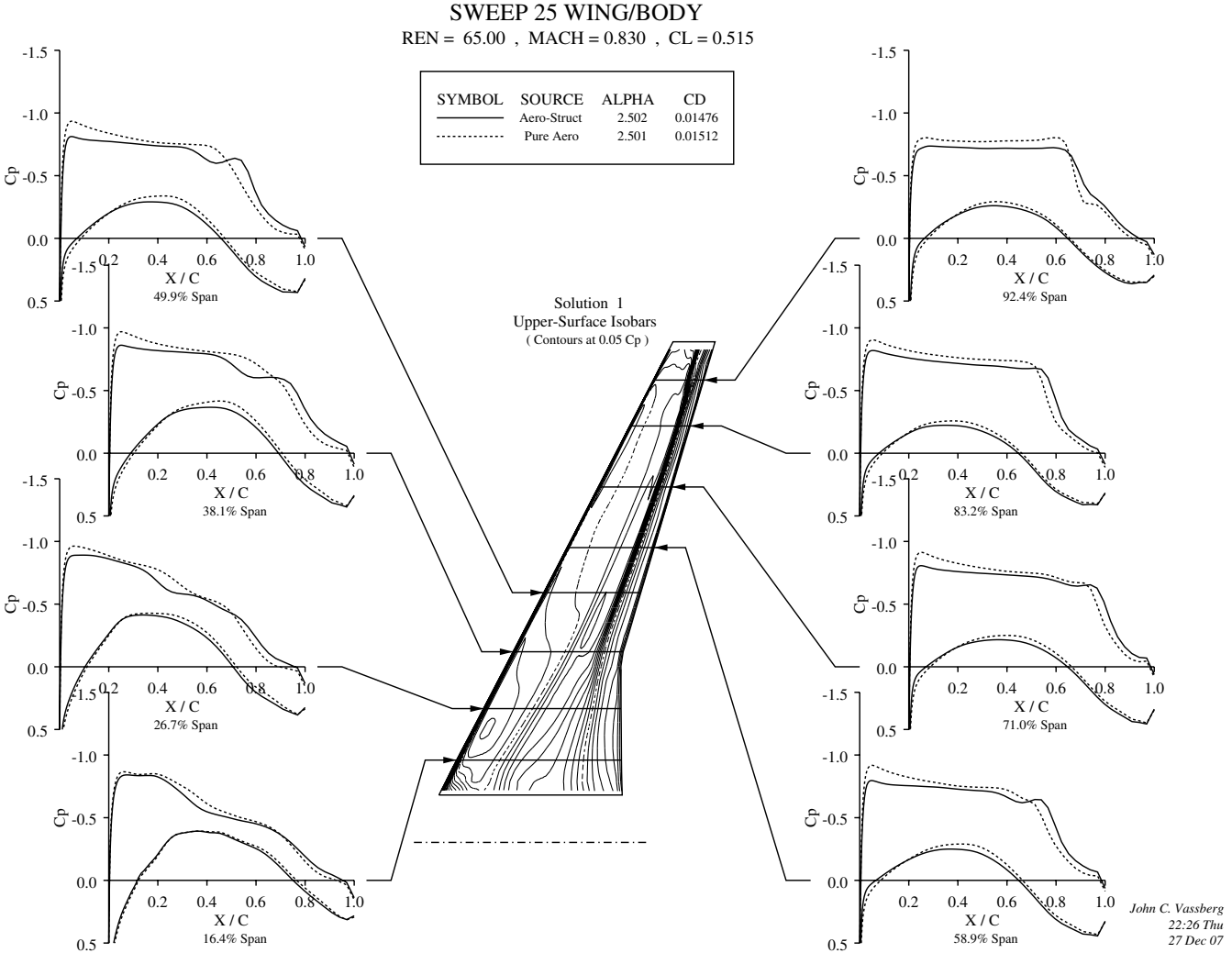

Fig. 8 Optimized design at Mach 0.83 and $\Lambda = 25°$.

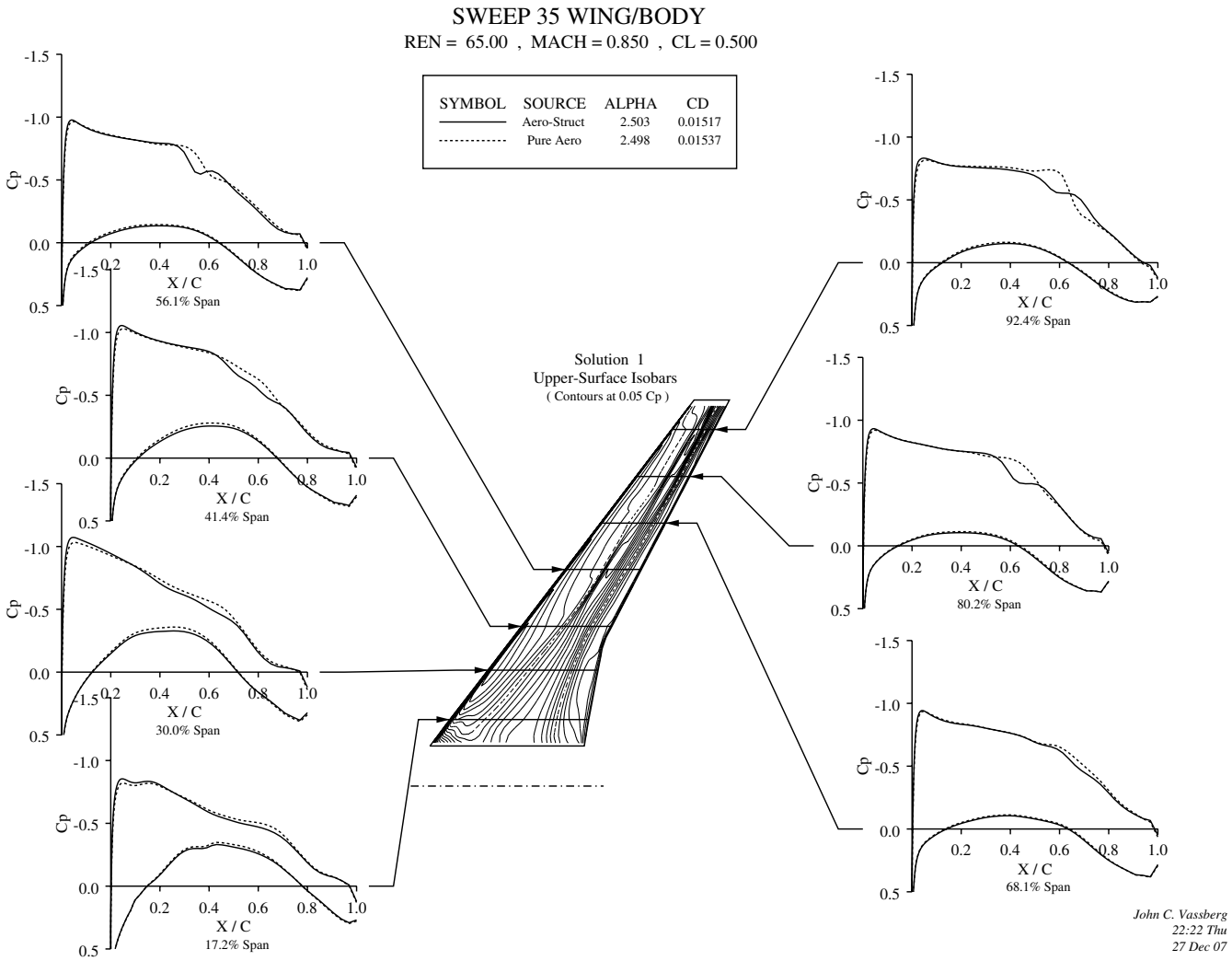

Fig. 9 Optimized design at Mach 0.85 and $\Lambda = 35°$.

$$I = \alpha_1 C_D + \alpha_2 \frac{1}{2} \int_{\mathcal{B}} (p - p_d)^2 \, \mathrm{d}S + \alpha_3 C_W \tag{2}$$

This form of the metric enables the designer to evaluate the tradeoffs between improvements in aerodynamic and structural performance. Furthermore, by varying the α vector, Pareto fronts can be established. The aerodynamic–structural optimization procedure is schematically depicted in Fig. 3, and the structural optimization is embedded as an inner loop in the overall design process.

The wing section is modeled by surface mesh points, and the wing planform is modeled by several global design variables, such as chord at various locations, span, sweepback, and wing-thickness ratio [13]. The structural model can be as detailed as desired, but presently includes the main wing box, ribs, and spars (Fig. 4). The calculations allow for optimization of both the sizes and layout of the structural elements under the wing loads and changes in the aerodynamic flow due to the wing deflection. A recent aerodynamic–structural redesign of a Boeing 747 wing using this approach, but with a lower-fidelity structural model, reduced the wing drag coefficient from $C_D = 0.0137$ to 0.0114 in 20 design cycles, with the wing lift coefficient fixed at $C_L = 0.45$, while simultaneously reducing the calculated wing weight by 1211 lb [14].

V. Results

Seven wing-body configurations were studied with varying sweep angles (35, 30, 25, 20, 15, 10, and 5°). The Mach number was systematically reduced from 0.85 for the highest-sweep wing to 0.79 for the lowest-sweep wing, and the lift coefficient was simultaneously increased to maintain MC_L roughly constant. Initial aerodynamic shape optimizations were performed on these configurations, subject to the constraint that thickness could not be reduced anywhere on the wing. The results of this study are summarized in Table 2. These optimizations show that the ML/D of the different configurations are all within 1.8% of the maximum value, suggesting a relatively flat design space for aerodynamic performance. Moreover, taking $\sqrt{M}L/D$ as a better approximation to range factor, this trend yields up to a 4% improvement, favoring the lower-swept wings. At the very least, these results show promise that reduced-wing-sweep designs are possible for efficient transonic cruise.

To illustrate the effectiveness of the aerodynamic shape optimizations performed herein, Fig. 5 provides the evolution of the pressure distributions for the $\Lambda = 10°$-sweep wing. Pressure distributions of the seed wing are depicted by the design-00 dashed-line curves. Also included are intermediate states for design cycles 10, 20, and 35 (the total number of design cycles was preset to 50). Pressure distributions of the final design are given by the solid-line curves of design-50. The seed wing exhibits very strong shocks over most of its span. During the evolution of this optimization, the shock system is monotonically reduced in strength, with the final design comprising only very weak shock waves. Note that the drag of the seed wing is 207.3 counts and that the drag of the final design is 157.3 counts; hence, the optimization reduced the wing drag by 50 counts: about 25% in this case. This represents a substantial enhancement in

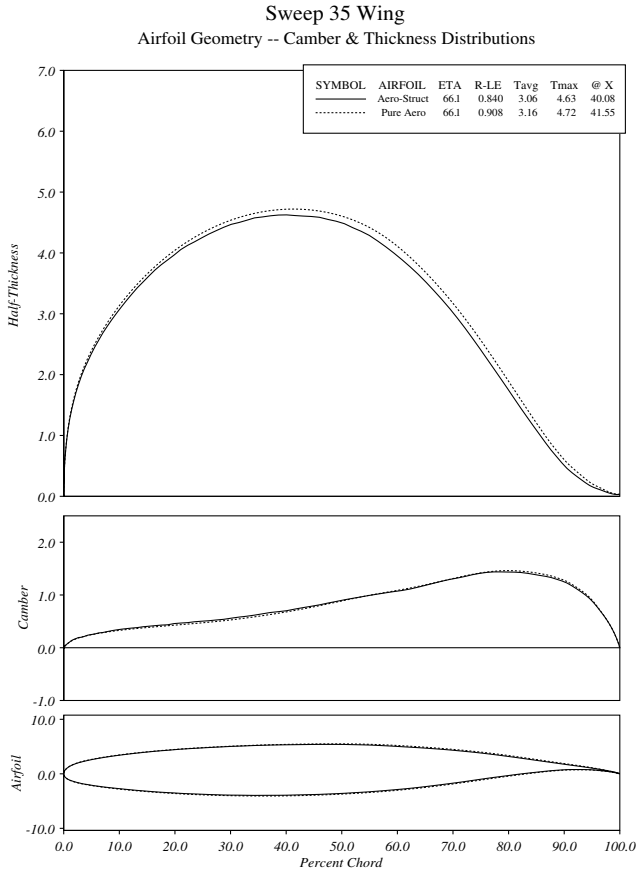

Fig. 10 Airfoil sections at $\eta = 66\%$ of optimal $\Lambda = 35°$ wing.

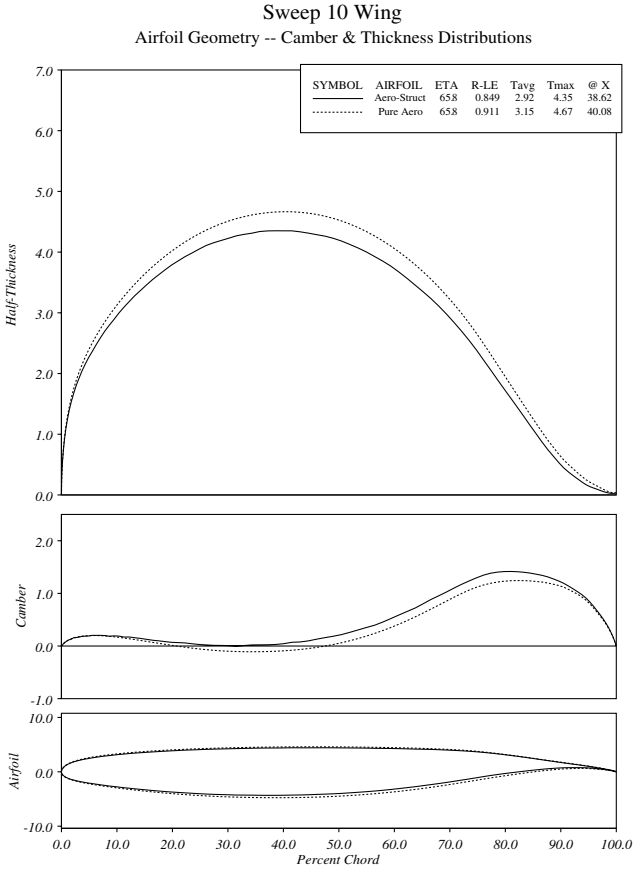

Fig. 11 Airfoil sections at $\eta = 66\%$ of optimal $\Lambda = 10°$ wing.

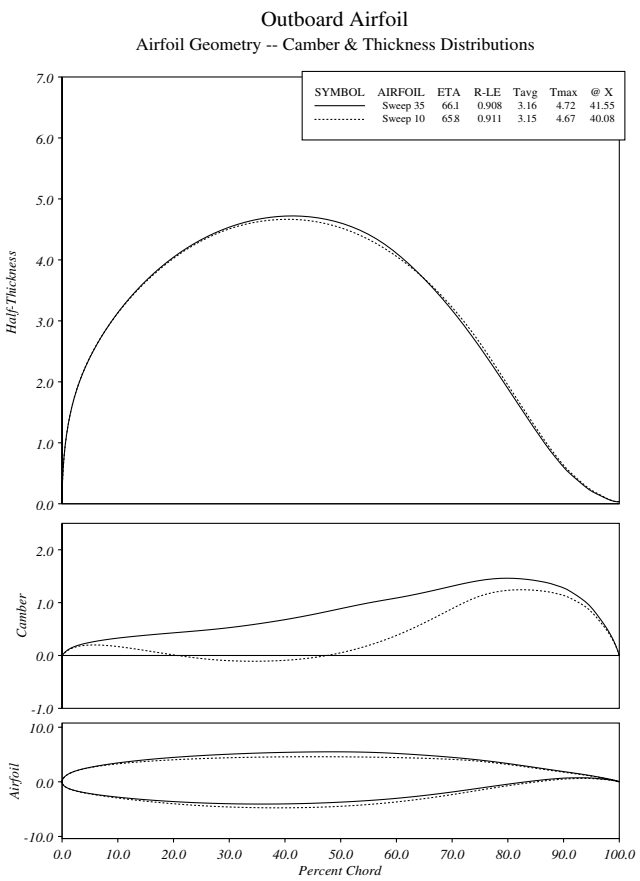

Fig. 12 Airfoil sections at $\eta = 66\%$ of optimal $\Lambda = 35°$ and $\Lambda = 10°$ wing.

aerodynamic performance that would most likely never be realized by a cut-and-try approach.

The wings obtained from the aerodynamic shape optimizations were then used in an aerodynamic–structural optimization procedure; this coupled method also allows for modest planform variations within limits set by the feasibility of morphing the mesh. The procedure is outlined in Fig. 3 and is a two-stage process. Following an aeroelastic simulation and an aerodynamic adjoint calculation, the structural elements are redesigned while holding the aerodynamic loads fixed. Once a structure with minimum weight is obtained that satisfies the stress constraints, the gradients for the airfoil points and the planform variables are determined to find the design that leads to an aerodynamic and structural performance improvement. With this new design, the sequence of aerodynamic–structural simulations and aerodynamic and structural adjoint calculations are repeated until a local minimum is determined.

The results of the aerodynamic–structural optimizations are summarized in Table 3. A similar behavior is observed for the different optimized designs. Figures 6–9 show the pressure distribution on a few of the wings with varying sweep used in this study. The aerodynamic performance is approximately the same and the structural weight is also roughly constant, suggesting that the aerodynamic–structural design space is also relatively flat. The planform variables of sweep and span, in particular, reveal interesting trends. The optimizer tended to slightly increase the sweep across the various configurations, whereas the span was slightly increased for the higher-sweep wings and slightly decreased for the lower-sweep cases. The aerodynamic–structural optimizations permit changes in the wing thickness; in fact, the thickness of the outboard wing was slightly reduced at the lower sweep angles, yielding a small reduction in shock drag that contributes to the trend of an increase in the range factor $\sqrt{M}L/D$ with reduced sweep. Similar to the pure aerodynamic optimizations, there is about a 4% improvement in range factor for the lowest-swept wing. The actual wing sections of the

optimized 35 and 10° swept wings are displayed in Figs. 10 and 11. Figure 10 shows that the primary difference between the aerodynamic–structural and pure aerodynamic optimizations for $\Lambda = 35°$ is in the thickness of the outboard airfoil sections near the critical station. Figure 11 illustrates that this trend for the $\Lambda = 10°$ case is more exaggerated. Just as interesting, varying the sweep for the pure aerodynamic optimizations has a dramatic effect on the airfoil camber distribution, as shown in Fig. 12.

In the studies summarized by Tables 2 and 3 the lift coefficient was varied to maintain a roughly constant MC_L, with the consequence that variations of ML/D are dictated by the value of C_D. In fact, the optimum cruising lift coefficient may vary with Mach number in a different manner. To address this question, we selected the $\Lambda = 10$ and 35° wings for further analysis. As shown in Tables 4 and 5, the lift-to-drag L/D ratios of both wings show an increasing trend as the lift coefficient is further increased. However, it is doubtful whether a practical design could operate at such high lift coefficients, for a variety of reasons. First, these results are for single-point optimizations, and when the design point is too extreme, it typically leads to a rapid degradation away from the design point. Second, the wing must be able to support a 1.3 g turn without experiencing buffet, and this sets a limit on the usable design lift coefficient. Third, very high lift coefficients may require an excessively high cruising altitude beyond the capability of the engines or may require a decrease in wing area with a consequent decrease in fuel volume.

VI. Conclusions

The results of this study suggest that it may be possible to design wings for commercial transport aircraft with low sweep without incurring either aerodynamic or structural performance degradations. Tables 2 and 3 show that whereas ML/D (which is a metric for aerodynamic efficiency) does not change much (around 0.5%) with decreased sweep, $\sqrt{M}L/D$ (which is a measure of specific fuel consumption) shows an improvement (around 4%) with decreased sweepback. However, these improvements are realized with an associated decrease in the cruising Mach number. On the other hand, on shorter-range routes (say, less than 1000 miles), the time savings of increasing the Mach number beyond 0.8 are negligible. The present design studies provide an indication that it might be better in this case to use a wing with reduced sweep, or a completely unswept wing, particularly when one takes account of the takeoff, climb, descent, and landing segments of the flight profile. On very long-range flights, the benefits of a reduction in flight time favor a swept wing with a higher cruising Mach number, even if there is no benefit in range efficiency. This suggests that other aspects of the design process (and business models) might dictate the choice of sweepback. For production and servicing reasons, it may be desirable to maintain commonality of the airframes for the short- and long-range missions, which would favor the choice of a swept wing.

Although the present investigation suggests improvements in aerodynamic efficiency with decreased sweepback, the authors feel that more detailed studies of complete configurations should be conducted to better quantify the magnitude of the potential benefits. For example, it would be beneficial to conduct similar exercises in collaboration with a larger and more diverse team of experts in a realistic airplane-design environment.

Acknowledgments

The aerodynamic optimization technologies used herein have greatly benefited from the long-term and continuing support of the U.S. Air Force Office of Scientific Research, Computational Mathematics Program directed by Fariba Fahroo. All computations were performed on the facilities of Intelligent Aerodynamics, including three 12-processor Orions and an HPC Box Cluster composed of four dual-core CPUs running at 3 GHz. The second author extends his appreciation to The Boeing Company for allowing his participation in this and other similar collaborations.

References

[1] Jameson, A., "Computational Aerodynamics for Aircraft Design," *Science*, Vol. 245, 1989, pp. 361–371. doi:10.1126/science.245.4916.361

[2] Jameson, A., "Aerodynamic Design via Control Theory," *Journal of Scientific Computing*, Vol. 3, 1988, pp. 233–260. doi:10.1007/BF01061285

[3] Jameson, A., "Optimum Aerodynamic Design Using Control Theory," *Computational Fluid Dynamics Review*, Wiley, New York, 1995.

[4] Jameson, A., "Efficient Aerodynamic Shape Optimization," AIAA Paper 2004-4369, Jan. 2004.

[5] Vassberg, J. C., and Jameson, A., "Aerodynamic Shape Optimization Part 1: Theoretical Background," *Introduction to Optimization and Multidisciplinary Design*, VKI Lecture Series, von Karman Inst. for Fluid Dynamics, Brussels, Belgium, March 2006.

[6] Jameson, A., and Vassberg, J. C., "Studies of Alternative Numerical Optimization Methods Applied to the Brachistochrone Problem," *CFD Journal*, Vol. 9, No. 3, Oct. 2000, pp. 281–296.

[7] Jameson, A., Martinelli, L., and Vassberg, J. C., "Using CFD for Aerodynamics—A Critical Assessment," *International Congress of Aerospace Sciences*, Toronto, Sept. 2002.

[8] Jameson, A., and Vassberg, J. C., "Computational Fluid Dynamics for Aerodynamic Design: Its Current and Future Impact," AIAA Paper 2001-0538, Reno, NV, Jan. 2001.

[9] Jameson, A., and Vassberg, J. C., "Aerodynamic Shape Optimization of a Reno Race Plane," *International Journal of Vehicle Design*, Vol. 28, No. 4, 2002, pp. 318–338. doi:10.1504/IJVD.2002.001993

[10] Vassberg, J. C., Page, G. S., Foch, R. J., and Jameson, A., "Aerodynamic Design and Optimization of the Mars Airborne Remote Exploration Scout," 42nd AIAA Aerospace Sciences Meeting and Exhibit, Reno, NV, AIAA Paper 2004-0401, Jan. 2004.

[11] Vassberg, J. C., and Jameson, A., "Aerodynamic Shape Optimization Part 2: Sample Applications," *Introduction to Optimization and Multidisciplinary Design*, VKI Lecture Series, von Karman Inst. for Fluid Dynamics, Brussels, Belgium, March 2006.

[12] Bendsoe, M. P., and Kikuchi, N., "Generating Optimal Strategies in Structural Design Using a Homogenization Method," *Computer Methods in Applied Mechanics and Engineering*, Vol. 71, No. 2, Nov. 1988, pp. 197–224. doi:10.1016/0045-7825(88)90086-2

[13] Leoviriyakit, K., "Wing Planform Optimization via an Adjoint Method," Ph.D. Thesis, Dept. of Aeronautics and Astronautics, Stanford Univ., Stanford, CA, Feb. 2006.

[14] Jameson, A., Leoviriyakit, K., and Shankaran, S., "Multipoint Wing Planform Optimization Using Control Theory," 45th AIAA Aerospace Sciences Meeting and Exhibit, Reno, NV, AIAA Paper 2007-0764, Jan. 2007.